Electronic Supplementary Information for

Photochemical reaction on graphene surfaces controlled by substrate-surface modification with polar self-assembled monolayers

Ryo Nouchi[a,b] and Kei-ichiro Ikeda[a]

[a] Department of Physics and Electronics, and Nanoscience and Nanotechnology Research Center, Osaka Prefecture University, Sakai 599-8570, Japan

[b] PRESTO, Japan Science and Technology Agency, Kawaguchi 332-0012, Japan

Contents:

- Supplementary text: Correction of Raman data.

Being the starting point of the data correction procedure, the origin of the coordinates in Fig. 3(a) in the main text, i.e., $\omega_{2D}{}^0$ and $\omega_G{}^0$, must be determined. Theses quantities have been reported to be 2676.9 and 1581.6 cm^{-1}, respectively, at an excitation laser wavelength of 514 nm.[1] In the present study, we used a Raman microscope equipped with a 532-nm laser. The 2D band is known to exhibit dispersive behaviour[2] and the wavenumber of the 2D band changes with the laser energy by 88 cm^{-1} eV^{-1}.[3] Thus, $\omega_{2D}{}^0$ in cm^{-1} for Raman characterization at an excitation laser wavelength of λ in nm can be expressed as:

$$\omega_{2D}{}^0 = 2676.9 + 88 \times \left(\frac{1240}{514} - \frac{1240}{\lambda}\right).$$

From this relationship, $\omega_{2D}{}^0$ for $\lambda = 532$ nm was determined to be 2669.7 cm^{-1}.

The determined origin $(\omega_G{}^0, \omega_{2D}{}^0) = (1581.6, 2669.7)$ [cm^{-1}] is now used in the vector decomposition analysis as shown in Fig. 3(a) in the main text. For the analysis, a transformation from the Cartesian to an oblique coordinate system is required. By defining the angle made by the strain axis (hole-doping axis) and the G-position axis as θ_y (θ_x), the transformation of the Cartesian coordinate of the point P (a, b) to the oblique coordinate (a', b') can be expressed as:

$$\begin{pmatrix} \Delta\omega_G \\ \Delta\omega_{2D} \end{pmatrix} \equiv \begin{pmatrix} a \\ b \end{pmatrix} = A \begin{pmatrix} a' \\ b' \end{pmatrix}, \qquad A \equiv \begin{bmatrix} \cos\theta_x & \cos\theta_y \\ \sin\theta_x & \sin\theta_y \end{bmatrix}.$$

$$\begin{pmatrix} a' \\ b' \end{pmatrix} = A^{-1} \begin{pmatrix} a \\ b \end{pmatrix},$$

$$A^{-1} = \frac{1}{\cos\theta_x \sin\theta_y - \cos\theta_y \sin\theta_x} \begin{bmatrix} \sin\theta_y & -\cos\theta_y \\ -\sin\theta_x & \cos\theta_x \end{bmatrix}.$$

For uniaxial strain, $\cos\theta_y = 1/\sqrt{1^2 + 2.2^2}$ and $\sin\theta_y = 2.2/\sqrt{1^2 + 2.2^2}$; for hole doping, $\cos\theta_x = 1/\sqrt{1^2 + 0.55^2}$ and $\sin\theta_x = 0.55/\sqrt{1^2 + 0.55^2}$; for electron doping, $\cos\theta_x = 1/\sqrt{1^2 + 0.2^2}$ and $\sin\theta_x = 0.2/\sqrt{1^2 + 0.2^2}$. Using the vector decomposition analyses, the as-measured wavelengths of the G and 2D bands can be converted to the $\Delta\omega_G$ value solely from the carrier doping effect (i.e., the $\Delta\omega_G$ value corresponding to no strain condition), $\Delta\omega_G{}^0$, as:

$$\Delta\omega_G{}^0 = a' \cos\theta_x$$

$$= \frac{\cos\theta_x}{\cos\theta_x \sin\theta_y - \cos\theta_y \sin\theta_x}\left(\Delta\omega_G \sin\theta_y - \Delta\omega_{2D} \cos\theta_y\right).$$

The obtained $\Delta\omega_G{}^0$ value can be related to the Fermi level relative to the Dirac point, E_F, as:[4]

$$E_F \gtrsim +100 \text{ meV (for electron doping)}, E_F = +21\Delta\omega_G{}^0 + 75,$$

$$E_F \lesssim -100 \text{ meV (for hole doping)}, E_F = -18\Delta\omega_G{}^0 - 83.$$

The $\Delta\omega_G{}^0$ values within $|E_F| \lesssim 100$ meV are nearly constant because of spatial fluctuations of E_F (i.e., electron–hole puddles[5, 6]), where the constant range depends on the sample quality. It should be noted that linear relationships only hold for $|E_F| \lesssim 500$–600 meV.[4]

1.   J. E. Lee, G. Ahn, J. Shim, Y. S. Lee and S. Ryu, *Nat. Commun.*, 2012, **3**, 1024.
2.   M. J. Matthews, M. A. Pimenta, G. Dresselhaus, M. S. Dresselhaus and M. Endo, *Phys. Rev. B*, 1999, **59**, R6585.
3.   D. L. Mafra, G. Samsonidze, L. M. Malard, D. C. Elias, J. C. Brant, F. Plentz, E. S. Alves and M. A. Pimenta, *Phys. Rev. B*, 2007, **76**, 233407.
4.   G. Froehlicher and S. Berciaud, *Phys. Rev. B*, 2015, **91**, 205413.
5.   E. H. Hwang, S. Adam and S. D. Sarma, *Phys. Rev. Lett.*, 2007, **98**, 186806.
6.   J. Martin, N. Akerman, G. Ulbricht, T. Lohmann, J. H. Smet, K. von Klitzing and A. Yacoby, *Nat. Phys.*, 2008, **4**, 144.
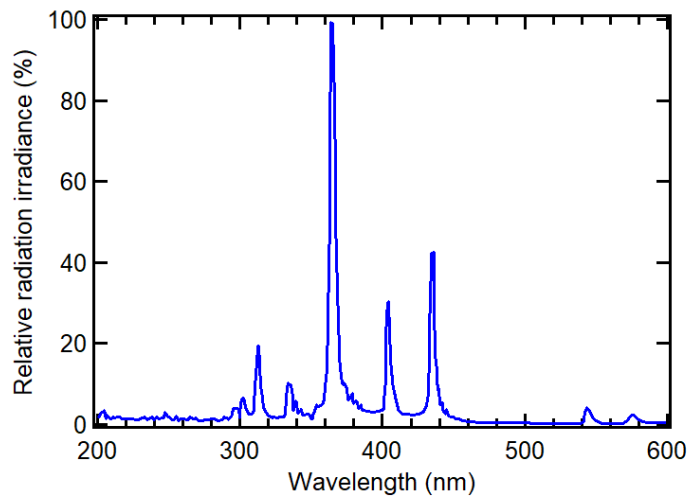
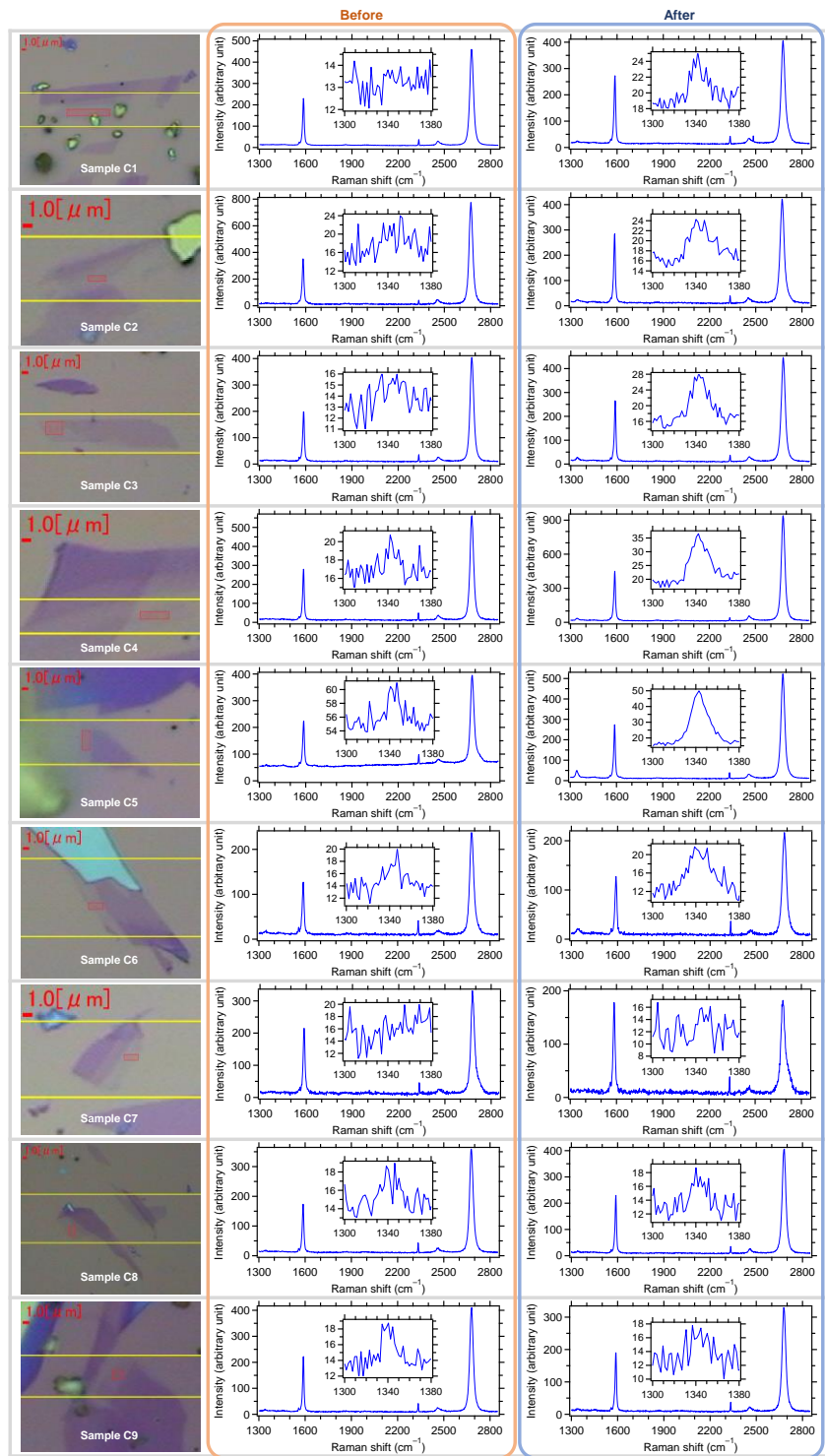**Fig. S1.** Emission spectrum from the ultraviolet light source used in this study.

Fig. S2. Raman scattering spectra acquired before and after the solid phase photochemical reaction of graphene on CH₃-SAM. Left panels show an optical micrograph, where Raman mapping was acquired in the region between two yellow lines and the red square region was used to obtain the averaged Raman spectra, shown in the center and right panels. Insets in the center and right panels are an enlarged view of the D band region.
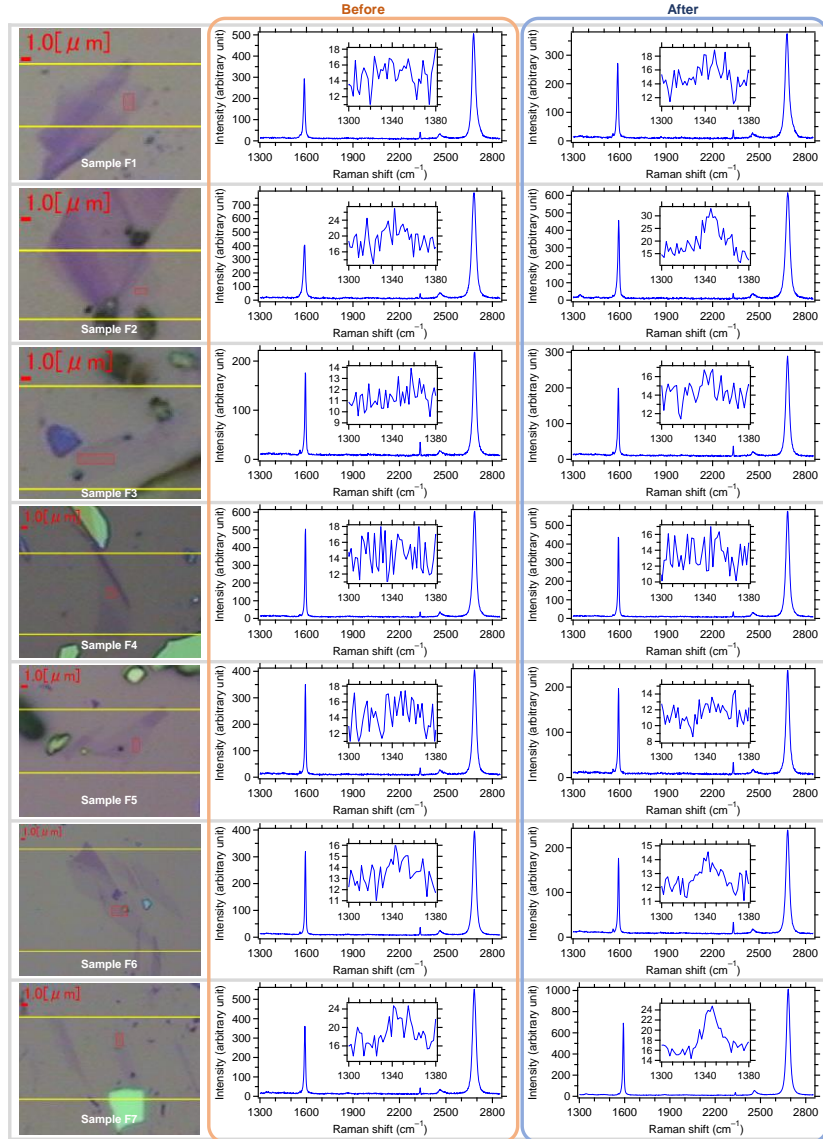
Fig. S3. Raman scattering spectra acquired before and after the solid phase photochemical reaction of graphene on F-SAM. Left panels show an optical micrograph, where Raman mapping was acquired in the region between the two yellow lines and the red square region was used to obtain the averaged Raman spectra, shown in the center and right panels. Insets in the center and right panels are an enlarged view of the D band region.
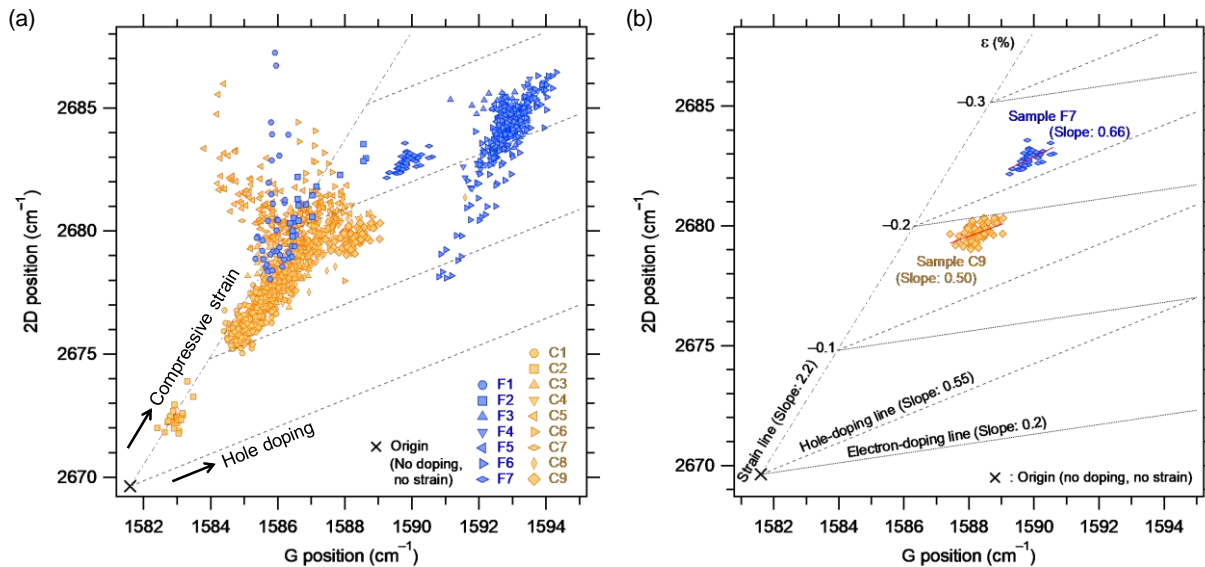
Fig. S4. 2D–G correlation including intra-flake variations. (a) All the measured flakes. (b) Flakes that showed a notable ω_G^{before} distribution with a straight fit line.
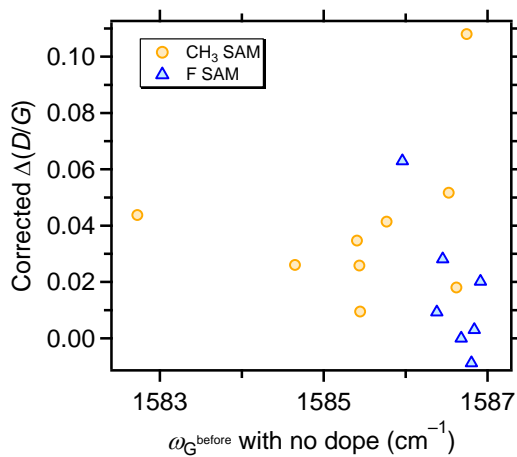

Fig. S5. Corrected relationship between the degree of the solid phase photochemical reaction and the G-peak wavenumbers solely determined by the strain level.
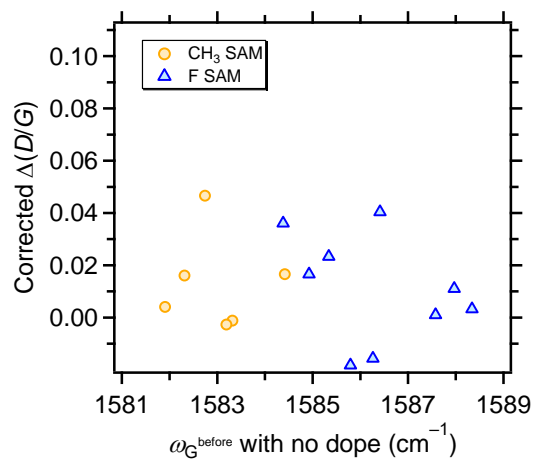
Fig. S6. Corrected relationship between the degree of the gas phase photo-oxidation and the G-peak wavenumbers solely determined by the doping level.